# Patient Specific Heart Models from High Resolution CT

Chandrajit Bajaj & Samrat Goswami & Zeyun Yu & Yongjie Zhang
Department of Computer Sciences,
Computational Visualization Center,
Institute of Computational Engineering and Sciences,
University of Texas at Austin,
Austin, Texas 78712

Yuri Bazilevs & Thomas Hughes
Department of Aerospace Engineering and Engineering Mechanics,
Institute of Computational Engineering and Sciences,
University of Texas at Austin,
Austin, Texas 78712

Computer Tomography (CT) and in particular super fast, 64 and 256 detector CT has rapidly advanced over recent years, such that high resolution cardiac imaging has become a reality. In this paper, we provide a solution to the problem of automatically constructing three dimensional (3D) finite-element mesh models (FEM) of the human heart directly from high resolution CT. Our overall computational pipeline from 3D imaging to FEM models has five main steps, namely, (i) discrete voxel segmentation of the CT (ii) discrete topological noise filtering to remove non-regularized, and small geometric measure artifacts (iii) a reconstruction of the inner and outer surface boundaries of the human heart and its chambers (iv) computation of the medial axis of the heart boundaries and a volumetric decomposition of the heart into tubular, planar and chunky regions, (v) a flexible match and fit of each of the decomposed volumetric regions using segmented anatomical volumetric templates obtained from a 3D model heart.

## 1 INTRODUCTION

Computer aided diagnosis and treatment of cardiovascular disease, in particular atherosclerosis, left ventricular hypertrophy, valvular dysfunction, increasingly rely on faithful patient specific heart FEM (finite element mesh) models that can be used in full-cycle simulation of pulsatile blood flow through the heart. An emerging methodology to construct spatially realistic human heart models is via super fast, 64 and 256 detector (high resolution) Computer Tomographic (CT) imaging (Toshiba Medical Systems - 64 Slice CT 2006).

Volume rendering of one such CT64 dataset is shown in Figure 2. Although state-of-the-art, the imaging is only the first step of a significant computational sequence of image and geometry processing steps, that are necessary for generating a robust and spatially realistic FEM model. In this paper, we present such a computational pipeline (see Figure 1) that processes the imaging data, and additionally uses an anatomically correct template heart 3D model, to construct an anatomically correct patient specific FEM model.
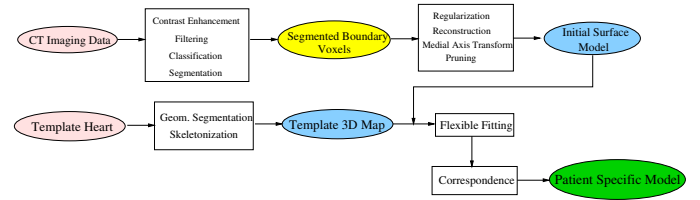


Figure 1: The Computational Pipeline

Our overall computational pipeline from 3D imaging to FEM models has five main steps, namely, (i) discrete voxel segmentation of the CT (ii) discrete topological noise filtering to remove non-regularized, and small geometric measure artifacts (iii) a reconstruction of the inner and outer surface boundaries of the human heart and its chambers (iv) computa-

tion of the medial axis of the heart boundaries and a volumetric decomposition of the heart into tubular, planar and chunky regions, (v) a flexible match and fit of each of the decomposed volumetric regions using segmented anatomical volumetric templates obtained from a 3D model heart. The pipeline has two major components. One path works on the imaging data, filters the noise, segments the main components of the heart and builds an initial surface mesh. As discussed in Section 2, this initial model is not always correct because of missing information and topological inconsistency. To circumvent that, we create a segmented 3D map from the template heart model and annotate it properly that helps build a correspondence with the initial and possibly incomplete model created from the imaging data. Further we match and fit the patient specific model with the segmented 3D map and inherit the information encoded there to fill up the gap of the missing information as well as remove the noisy spurious components that could not be avoided due to ambiguity in the imaging data. Figure 6 (a) shows the template model used in this paper.

Section 2 discusses the steps necessary to build the initial heart model from the imaging data. Section 3 discusses the steps necessary to build the template segmented 3D map. Finally, in Section 4, we discuss the tasks that are needed to accomplish to finally obtain the patient specific model of heart.
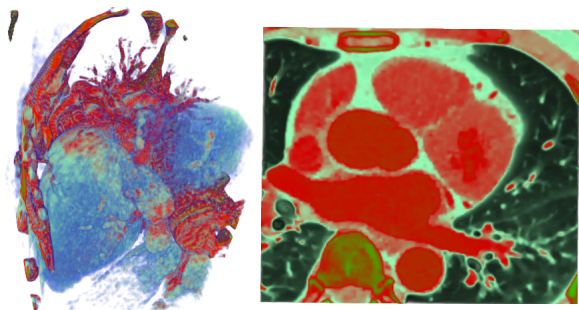


Figure 2: Left subfigure shows the volume rendering of a subvolume of the input CT imaging data. Right subfigure shows a portion of the cross-section of the input. One full slice is shown in the two leftmost subfigures in Figure 3.

## 2   PATIENT SPECIFIC DATA PROCESSING

In this section, we discuss the issues that need to be tackled in order to process the imaging data effectively. In the following subsections, we discuss the four main steps, namely *Segmentation or Classification*, *Regularization*, *Reconstruction* and *Pruning*. Additionally, in each of these subsections, we show the results of each of these steps on an imaging dataset. The dataset is courtesy Dr. Char-

lie Walvaert of Austin Heart Hospital. The imaging dataset is of dimension $512 \times 512 \times 432$ and the spacing in $x, y, z$ directions are respectively $0.390625mm, 0.390625mm, 0.3mm$.

### 2.1   Image Segmentation

Segmentation is a way to dissect the features of interest from their surroundings. In case of the heart dataset, we aim to extract the four chambers automatically. To this end, we have developed a computational procedure based on the fast marching method (Sethian 1996; Malladi and Sethian 1998; Sethian 1999). In this method, a contour is initialized from a pre-chosen seed point, and the contour is allowed to grow until a certain stopping condition is reached. The traditional fast marching method is designed for single object segmentation. In order to segment multiple objects, like the chambers in the heart data, a seed for each of the components must be chosen. When contours from different seed points, they should stop each other on their boundaries. This multi-seeded fast marching method (Yu and Bajaj 2005; Sifakis and Tziritas 2001) simultaneously segment all the components and hence is extremely useful to separate multiple features that are too close to segment sequentially.
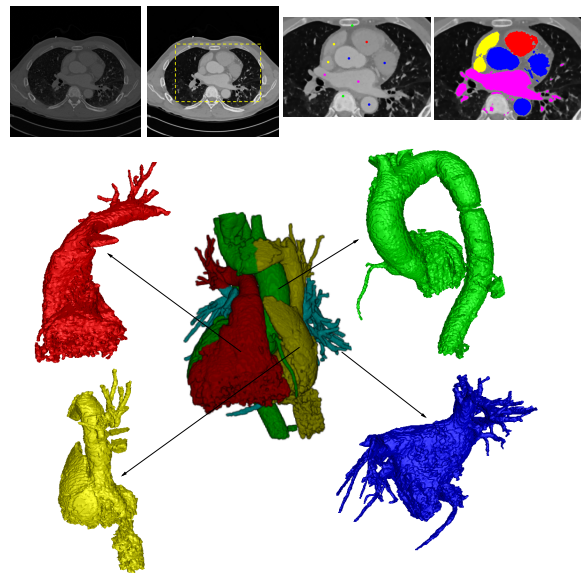


Figure 3: Top row shows the slice of the input image, the result after contrast enhancement and anisotropic filtering, seed selection for segmentation and finally the result of segmentation process on that single slice. The second row shows the overall segmentation of the imaging data into four subvolumes. The dissociation is enhanced by coloring it differently. The subfigures show the exploded view of the individual subvolumes.

Since the given patient-specific heart data is very noisy and has a low contrast, it is always useful to filter the noise and enhance the contrast before we segment the features of interest. We have developed

a fast and adaptive method for contrast enhancement (Yu and Bajaj 2004), which was applied to the given heart data. Additionally, an anisotropic noise reduction approach (Perona and Malik 1990; Bajaj, Wu, and Xu 2003) was employed to smooth out the noise as seen in the original data. Compared to the isotropic (e.g., Gaussian) filtering methods, the anisotropic approaches can preserve sharp features much better while the noise is reduced. Figure 3 shows the result of image segmentation on the imaging data.

## 2.2 Regularization

This step is optionally employed to remove the artifacts of the voxel-based classification. The level-set based segmentation can involuntarily produce voxels which are, although connected, can be thought of as dangling components. Such spurious subset of voxels pose problem in reconstructing a surface out of the boundary voxels. Therefore a careful selection/removal of a subset of voxels output by the segmentation step is crucial. The result of this step is a set of boundary voxels whose centers lie on the surface of the segmented boundary with all dangling components removed. In our experiments, we have not encountered such cases with the dataset that we dealt with. Nevertheless, this step should optionally be included in the pipeline for curation of the segmented region boundaries.
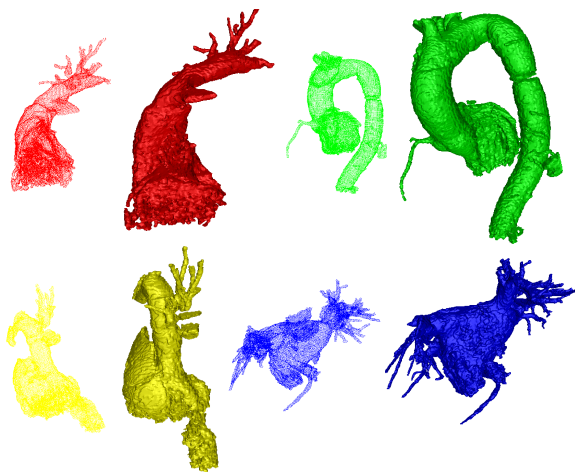
## 2.3 Reconstruction



Figure 4: Reconstruction of four segmented boundaries of the patient specific heart. With each surface mesh the corresponding pointset is shown in the same color.

From the regularized voxel centers, we reconstruct the surface that faithfully depict the surface triangle mesh of the boundary in question. There are number of reconstruction technique available for this purpose (Bajaj, Bernardini, and Xu 1995; Amenta and Bern

1999). For our purpose we use the *TightCocone* algorithm by (Dey and Goswami 2003). Sometimes, the noise present in the data is a major challenge to deal with and to circumvent that problem we employ the version of that algorithm that deals with noisy point cloud - *RobustCocone* (Dey and Goswami 2004).

This step results in the surface meshes which are good candidates for further fitting operation. The reconstructed surfaces of the components for the dataset is shown in Figure 4. As apparent from the pictures, the reconstructed surface contains several portions which are noisy and also some blood vessels which should not be used for matching the patient specific data with the template atlas. In the next subsection we describe that step.
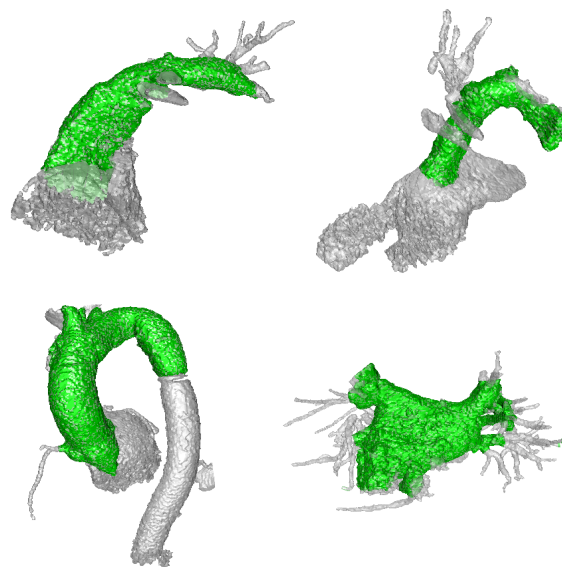
## 2.4 Pruning



Figure 5: Result of pruning: The green portions in each of the four extracted components contains reliable information that can be used to match the patient specific data with the template model. The missing or spurious portions of each component are drawn in white.

The quality of the imaging data is the main bottleneck in the modeling procedure and therefore it is necessary to clean-up the data before building the correspondence with the template atlas. The goal of this step is to identify the portions of the patient heart data which are missing and also the spurious components erroneously classified in the segmentation process because of weak intensity variation. We employ the geometry segmentation approach on the regularized pointset to achieve this goal. The segmentation approach, as described in (Dey, Giesen, and Goswami 2003), relies on a parameter which determines if two adjacent maxima should be clustered together and

form a bigger segment. Choosing this parameter carefully removes the small spurious components as well as the noisy incomplete portions of the patient heart models. Figure 5 shows the result of this step.

After this step we have a weaker annotation of the parts of the patient specific heart models - the ones which are stable and can be used for correlation with the atlas; and the ones which are either spurious or incomplete. The segments belonging to the second class can not be used for building correspondence with the template parts.

## 3 TEMPLATE PREPARATION

The patient specific imaging data is often incomplete and contains topologically inconsistent and spurious components. We rectify such anomalies by inheritance of topology from the template heart model. In order to do so, we first process the template geometry and annotate it following the heart anatomy. We call the template geometry $T$, which has two distinct components - $T_{out}$ and $T_{in}$. The analog of $T_{in}$ in the patient data is the inner wall of the heart which interfaces with the blood being circulated and the analog of $T_{out}$ is the outer boundary where the heart is embedded among soft tissues and muscles. Below we describe the major steps in processing the solid bounded by $T_{in}$, and construct a segmented 3D map of the template geometry which is key to inherit the topological and anatomical information into the patient specific imaging data.

### 3.1 Geometry Segmentation

Given $T_{in}$, we decompose it into 4 connected components -

1. Left Atrium - $T_{LA}$

2. Left Ventricle - $T_{LV}$

3. Right Atrium - $T_{RA}$

4. Right Ventricle - $T_{RV}$

Left and right ventricles are additionally segmented into the valves and aortic arches.

The key ingredient in this segmentation process is the careful analysis of the critical points of the distance function induced by each $T_*$.

Given any shape $S$, one can define a distance function $h_S : \mathbb{R}^3 \to \mathbb{R}$ which assigns to every point in the three dimensional space its distance to the nearest point on the object $S$. The function $h_S$ can be approximated by a similar function $h_P$ when $S$ is known only via a finite set of points $P$ sampled from $S$. This function, which is popularly known as *distance function* has a rich history of application and especially the critical point structure of this function encodes a lot of information about the shape attributes of $S$. For

a list of prior work, and especially on the topological invariants of the critical point structure, see (Bajaj, Bernardini, and Xu 1995; Edelsbrunner 2002; Giesen and John 2003).

For the purpose of segmentation, we use the partition of space by gradient uniformity which is otherwise known as the *stable manifold* of the critical points. The stable manifolds are computed efficiently via the Voronoi-Delaunay diagram of the pointset $P$. Details are given in (Dey, Giesen, and Goswami 2003).
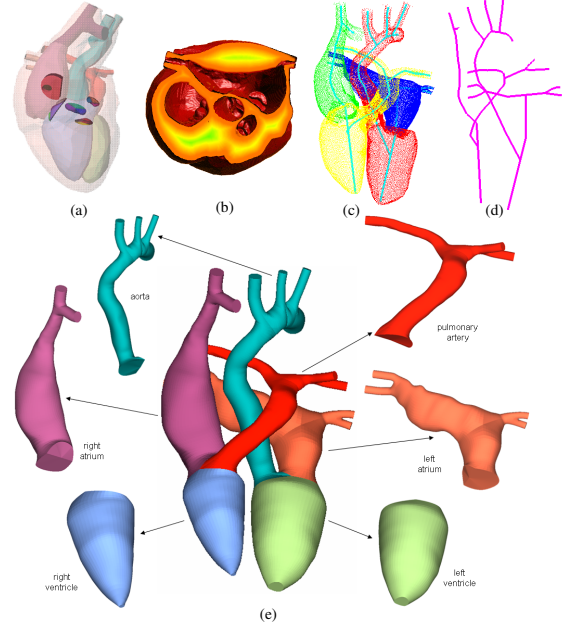


Figure 6: (a) Template model of human heart. The inner boundary is shown inside the transparent outer boundary of heart. (b) A cross section through the middle that is colored according to the value of the Signed Distance Function. (c) The skeleton of all four chambers (colored cyan). (d) Only the skeleton to help visualize the connectivity structure. (e) Complete segmented template 3D map.

### 3.2 Annotation

In the context of shape attributes, it is often required to annotate the decomposed parts as *tubular* or *flat* or *blobby*. Such annotation also can be performed via careful analysis of the critical point structure of $h_P$. The key ingredient to achieve this is a construct analogous to stable manifold, *unstable manifold*. These are partitions of space in accordance with negated gradient uniformity. It was shown in (Goswami, Dey, and Bajaj 2006), that unstable manifold of the index 1 and 2 saddle points reveal the *flat* and *tubular* features respectively. For our purpose, we apply the annotation process on every decomposed part.

As the Figure 6 (c,d) shows, the unstable manifold of the index 2 saddle points additionally produces the

4

skeleton of the object. For tubular regions, the skeletons are particularly useful as they can be used to fit a NURBS model as was done previously by (Zhang, Bazilevs, Goswami, Bajaj, and Hughes 2006).

### 3.3    Template Segmented 3D Map Creation

The process of segmentation and feature annotation create a complete description of the template which we call a *Template Segmented 3D Map*. This segmented 3D Map has different components of the model heart properly decomposed and tagged with domain knowledge of heart anatomy as to which component corresponds to which ventricle or aortic arch or atrium etc. We show the prepared atlas in Figure 6.

Once the template map is created, we build a correspondence table as to which part of the segmented patient data should be matched with which part of the segmented template. Figure 7 shows the correspondence.
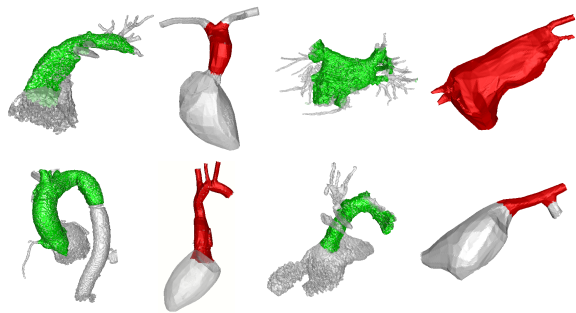


Figure 7: Correspondence between the informative components of the patient specific heart (green) and the template model (red). Every green part from the initial patient model is matched with the red part of the template.

## 4    CONCLUSION AND FUTURE WORK

In this paper, we have presented our current status of ongoing work on creating a patient specific model of heart from high resolution CT imaging data. We have developed a pipeline and described the steps that constitute the pipeline.

The remaining step is to fit the solids from the template atlas to the pruned components of the patient heart flexibly without violating the topological invariants of the template that conform with the heart anatomy. The template provides the invariant which, after the flexible fitting is performed, shall help fill up the missing information in the image and also remove the extraneous components from the model faithfully.

# REFERENCES

Amenta, N. and M. Bern (1999). Surface reconstruction by voronoi filtering. *22*(4), 481–504.

Bajaj, C., F. Bernardini, and G. Xu (1995). Automatic reconstruction of surfaces and scalar fields from 3D scans. In *ACM SIGGRAPH*, pp. 109–118.

Bajaj, C., Q. Wu, and G. Xu (2003). Level-set based volumetric anisotropic diffusion for 3d image denoising. In *ICES Technical Report, University of Texas at Austin*.

Dey, T. K., J. Giesen, and S. Goswami (2003). Shape segmentation and matching with flow discretization. In F. Dehne, J.-R. Sack, and M. Smid (Eds.), *Proc. Workshop Algorithms Data Strucutres (WADS 03)*, LNCS 2748, Berlin, Germany, pp. 25–36.

Dey, T. K. and S. Goswami (2003). Tight cocone: A water-tight surface reconstructor. In *Proc. 8th ACM Sympos. Solid Modeling and Applications*, pp. 127–134.

Dey, T. K. and S. Goswami (2004). Provable surface reconstruction from noisy samples. In *Proc. 20th ACM-SIAM Sympos. Comput. Geom.*, pp. 330–339.

Edelsbrunner, H. (2002). Surface reconstruction by wrapping finite point sets in space. In B. Aronov, S. Basu, J. Pach, and M. Sharir (Eds.), *Ricky Pollack and Eli Goodman Festschrift*, pp. 379–404. Springer-Verlag.

Giesen, J. and M. John (2003). The flow complex: a data structure for geometric modeling. In *Proc. 14th ACM-SIAM Sympos. Discrete Algorithms*, pp. 285–294.

Goswami, S., T. K. Dey, and C. L. Bajaj (2006). Identifying flat and tubular regions of a shape by unstable manifolds. In *Proc. 11th Sympos. Solid and Physical Modeling*, pp. 27–37.

Malladi, R. and J. Sethian (1998). A real-time algorithm for medical shape recovery. In *IEEE International Conference on Computer Vision*, pp. 304–310.

Perona, P. and J. Malik (1990). Scale-space and edge detection using anisotropic diffusion. *IEEE Trans. on Pattern Analysis and Machine Intelligence 12*(7), 629–639.

Sethian, J. (1996). A marching level set method for monotonically advancing fronts. *Proc. Natl. Acad. Sci. 93(4)*, 1591–1595.

Sethian, J. (1999). *Level Set Methods and Fast Marching Methods, 2nd edition*. Cambridge University pPress.

Sifakis, E. and G. Tziritas (2001). Moving object localization using a multi-label fast marching algorithm. *Signal Processing: Image Communication 16*(10), 963–976.

Toshiba Medical Systems - 64 Slice CT (2006, July). Clinical advancement in volumetric CT.

Yu, Z. and C. Bajaj (2004). A fast and adaptive algorithm for image contrast enhancement. In *Proc. IEEE International Conference on Image Processing*, pp. 1001–1004.

Yu, Z. and C. Bajaj (2005). Automatic ultrastructure segmentation of reconstructed cryo-em maps of icosahedral viruses. *IEEE Transactions on Image Processing: Special Issue on Molecular and Cellular Bioimaging 14*(9), 1324–1337.

Zhang, Y., Y. Bazilevs, S. Goswami, C. L. Bajaj, and T. J. R. Hughes (to appear 2006). Patient-specific vascular nurbs modeling for isogeometric analysis of blood flow. In *Proc. 15th Int. Meshing Roundtable*.